Nanotechnology **19** (2008) 255706 (7pp) doi:10.1088/0957-4484/19/25/255706

Gas sensing properties of tin oxide nanostructures synthesized via a solid-state reaction method

E T H Tan[1], G W Ho[1,2], A S W Wong[3], S Kawi[4] and A T S Wee[5]

[1] Department of Electrical and Computer Engineering, National University of Singapore, 4 Engineering Drive, 117576, Singapore
[2] Engineering Science Programme, National University of Singapore, 9 Engineering Drive 1, 117576, Singapore
[3] Institute of Materials Research and Engineering, A*STAR (Agency for Science, Technology and Research), 3 Research Link, 117602, Singapore
[4] Department of Chemical and Biomolecular Engineering, National University of Singapore, 4 Engineering Drive 4, 117576, Singapore
[5] Department of Physics, Surface Science Laboratory, National University of Singapore, 2 Science Drive 3, 117542, Singapore

E-mail: elehgw@nus.edu.sg (G W Ho)

Received 8 December 2007, in final form 8 March 2008
Published 15 May 2008
Online at stacks.iop.org/Nano/19/255706

Abstract
A high-yield synthesis of SnO_2 nanoparticles via a facile, economical and easily scalable solid-state molten salt synthesis method has been demonstrated. The inorganic additive, molar ratios of chemicals and annealing temperature were found to control the size and porosity of the SnO_2 nanoparticles. The synthesized SnO_2 nanostructures were uniform, well dispersed and exhibited high crystallinity. Hydrogen sensors made from the SnO_2 nanoparticles were found to possess high sensitivity and stability. Other than tailoring the material's structure in terms of size and porosity, another potential method of enhancing the gas sensitivity is functionalization with noble Pd metal.

1. Introduction

There is a growing need for hydrogen sensors in many areas such as chemical and petroleum refining, semiconductor processing for microelectronics, and biomedical applications [1]. In view of this, there is a need to develop a hydrogen sensor that possesses superior sensing properties such as high sensitivity, and fast response and recovery times, as well as the ability to operate optimally at a sufficiently low operating temperature. Many approaches have been researched to synthesize and develop effective hydrogen sensors, and most of the currently offered hydrogen sensors are based on metal oxides due to their superior hydrogen sensing properties. Among these metal oxides, stannic oxide (SnO_2) has been identified as one of the preferred materials because of its excellent gas sensing properties. SnO_2 nanostructure based sensors have been reported to show good sensitivity properties such as low detection limit, good selectivity, and short response and recovery time [2].

By using chemical processing, large amounts of easily processable SnO_2 nanoparticles can be obtained using mild conditions. For this reason, an increasing number of reports have been published on the chemical synthesis of oxide nanoparticles; the more common ones include sol–gel [3], spray-pyrolysis [4], solvothermal [5] and microwave methods [6]. Although low-dimensional tin oxide nanostructures have been prepared by several techniques, synthesizing tin oxide nanostructures in an economical, large-scale and efficient manner without the involvement of organometallic precursors and complex processes remains an issue. Our work employs the use of a solid-state reaction method to synthesize SnO_2 nanostructures in an economical, easily scalable and high-yield process. We have noted that our synthesis procedures closely resemble those of Sun *et al* [7]. In the solid-state synthetic route, reactions are usually initiated by self-initiation via grinding and/or annealing of the mixed reagents. The solid-state reaction has several unique features: the reaction can be self-initiated at room temperature, and internally produced heat can be self-sustained to produce crystalline products [8]. Thus by designing a reaction that involves the inclusion of appropriate additives

and the formation of desired by-products, it is possible to maximize the heat generated in the reaction, causing it to become a self-initiated one. The alkali halide NaCl is usually selected to be the by-product or additive because it is known to be an effective metal halide for a self-initiated reaction and it is stable against any undesired complex chemical reaction; it also possess sufficient aqueous solubility, which eliminates contamination issues in the end product [8]. The reaction is somewhat exothermic, such that heat released is sufficient to melt the halide salt additive or by-product to form a melt. In essence, the diffusion in the solid-state reaction is known to be short range, so the nucleated atoms or molecules are limited in a short range, thus forming nanosized particle.

In this paper, we report the effect of various reaction parameters that control the morphology and structure of the SnO_2 nanoparticles. In addition, the hydrogen sensing properties of SnO_2 nanostructures of various dimensions were investigated. Instead of changing the material structure in terms of size and porosity, a possibly superior method of enhancing the gas sensing properties via functionalization with noble Pd metal has shown great potential in gas sensitivity improvement.

2. Experimental details

2.1. Synthesis and characterization

The sample preparation procedure involved a facile and low-cost solid-state reaction method [7]. Fine SnO particles were first synthesized by a solid-state reaction of tin chloride dihydrate ($SnCl_2{\cdot}2H_2O$) and sodium hydroxide (NaOH). The $SnCl_2{\cdot}2H_2O$ (2.26 g, 10 mmol, AR grade) and NaOH (0.08 g, 20 mmol, AR grade) were ground with a mortar and pestle for 15 min. Next, sodium chloride (NaCl) was added to the mixture at a molar ratio of 1:2 and further ground for another 30 min. The mixture was then oxidized and annealed for 2 h at 400 °C. The final products were washed with water and dried for 2 h at 60 °C. This synthesis method produced a high yield (90% mass recovery) of SnO_2 nanoparticles. The parameters affecting the size and morphology of the synthesized SnO_2 nanostructures via the solid-state reaction method were investigated by varying various experimental conditions. Samples S1 and S2 were prepared by changing the amount of NaOH to 10 mmol and 40 mmol, respectively. Samples S3 and S4 were prepared by using a precursor to NaCl additive ratio of 1:1 and 1:4, respectively. Sample S5 was prepared by replacing the tin chloride dihydrate ($SnCl_2{\cdot}2H_2O$) by tin chloride pentahydrate ($SnCl_4{\cdot}5H_2O$). Samples S6 and S7 were prepared by annealing the mixture for 2 h at 350 and 800 °C, respectively. Note that in each case the other parameters were kept constant.

The morphology and structure of the nanostructures were characterized using a scanning electron microscope (SEM: JSM-6700F) operating at 10 kV and a transmission electron microscope (TEM: JEOL-2100) with an accelerating voltage of 300 kV. The energy-dispersive x-ray (EDX) elemental analysis was carried out using a JED-2300 EDX system fitted to the TEM. X-ray diffraction (XRD) was carried out using a Bruker general area detector diffraction system (GADDS) x-ray diffractometer with a two-dimensional (2D) detector at 40 mA and 40 kV using Cu Kα radiation ($\lambda = 1.541$ Å). X-ray photoelectron spectroscopy (XPS) was done using a VG ESCALAB MK2 equipped with an Mg Kα x-ray source operating at 300 W. Photoluminescence (PL) analysis was performed using an Accent Rapid PL Mapping System RPM 2000 He–Cd laser (325 nm and 1.8 mW). Brunauer–Emmett–Teller (BET) measurements were conducted using a surface area and pore analyzer (Quantachrome Autosorb-1 NOVA 1000) with N_2 as the adsorbate at liquid nitrogen temperature.

2.2. Hydrogen sensing

The synthesized SnO_2 powders were processed into pellet form to facilitate analysis of its response to H_2 gas. Individual pellets were created by adding 0.5 g of the SnO_2 powder into a custom-made pellet mould, and applying a pressure of 15 tons on the mould for at least 30 min thereafter. Platinum wires were embedded in the pellet samples for resistance measurement purposes. The Pd was coated on the surface of the pellet sensors using a Denton magnetron sputtering system at a base pressure of 10^{-6} Torr with a power of 100 W for a duration of 5 s. The sensitivity of the sensor was measured by the resistance changes during air and hydrogen gas cycling. The expression for sensor sensitivity to hydrogen is given as the ratio of the resistance in air to that in hydrogen ($S = R_{\text{air}}/R_{\text{hydrogen}}$).

3. Results and discussion

3.1. Synthesis and characterization

Figure 1(a) shows an SEM image of the SnO_2 nanoparticles grown by the solid-state reaction based on the reference conditions. The SnO_2 nanoparticles are spherical, uniform, well dispersed and show no aggregates in large visual fields. Figure 1(b) shows a complementary low-resolution TEM image of the SnO_2 nanoparticles dispersed on a copper grid. The size distribution of the nanoparticles is 20–80 nm.

The high-resolution TEM image (figure 1(c)) shows distinct lattice fringes. From figure 1(c) inset, the interplanar spacing is measured to be ∼0.251 nm, consistent with that for (200) rutile SnO_2. The TEM EDX spectrum (figure 1(d)) of the nanoparticles reveals that tin and oxygen are the only components present. No sodium and/or chlorine contamination was found in the product. From the quantitative TEM EDX analysis, the amount of oxygen is found to be approximately 62.8% while that of tin is about 37.2%. The oxygen element component is observed to be almost twice that of tin, hence confirming the chemical composition to be SnO_2.

Figure 2 shows the XPS results of the synthesized nanoparticles obtained at room temperature. The binding energy positions for all the elements were corrected with respect to C 1s at 284.6 eV. The Sn 3d spectrum (figure 2(a)) comprises two peaks with binding energies at 487.0 and 495.3 eV, which can be attributed to Sn $3d_{5/2}$ and Sn $3d_{3/2}$, respectively, in the form of tin oxide [9]. Figure 2(b) shows the O 1s spectrum; its asymmetric peak was fitted by two

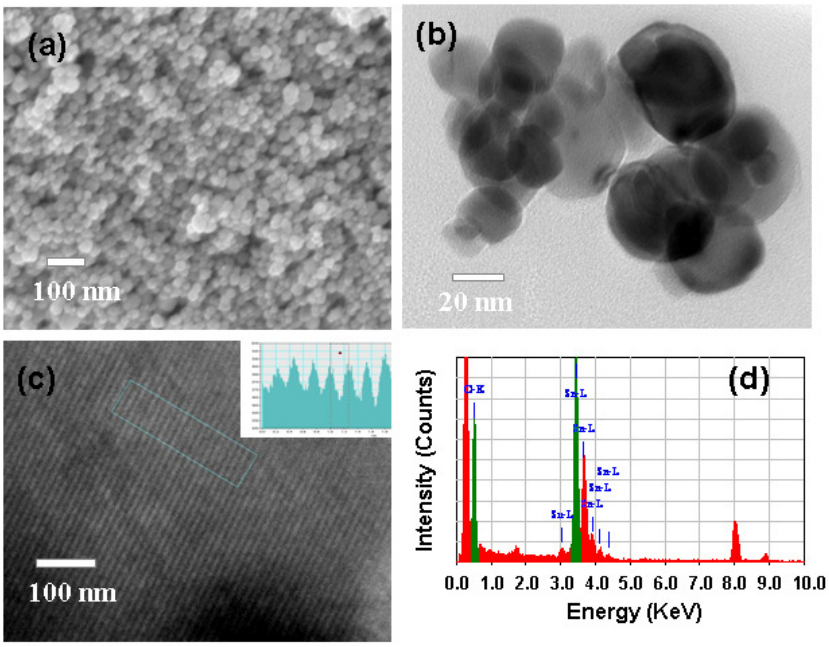

Figure 1. (a) SEM image of tin oxide nanoparticles produced under the reference conditions. (b) Low-resolution TEM image and (c) high-resolution TEM image of tin oxide nanoparticles; the inset shows the measured interplanar distance. (d) TEM EDX spectrum, showing the chemical composition of the nanoparticles produced.

(This figure is in colour only in the electronic version)

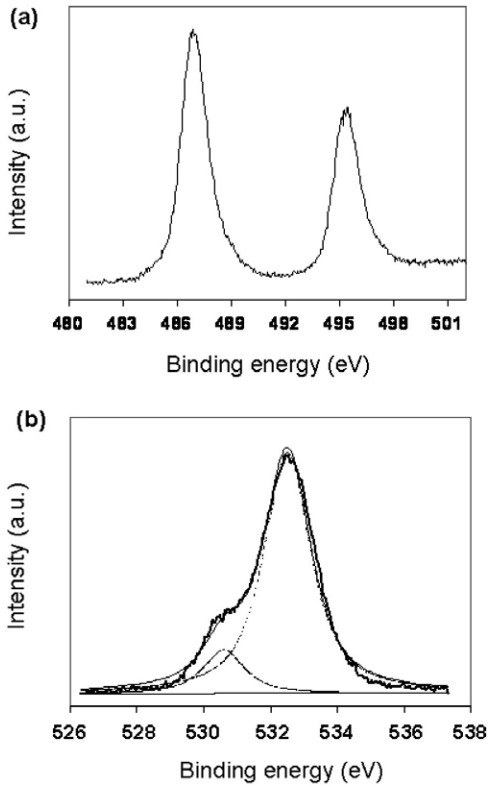

Figure 2. XPS spectra of (a) Sn 3d and (b) O 1s obtained from the synthesized nanoparticles.

components with binding energies at 531.0 and 532.5 eV. The respective peaks can be attributed to oxygen in SnO_2 and the SiO_2 substrate [10].

The effects of various parameters on the morphology of the SnO_2 nanoparticles were investigated. It was found that the dimension of the nanoparticles can be controlled by varying the precursor chemical ratio ($SnCl_2{\cdot}2H_2O$:NaOH), precursor to NaCl additive ratio ($SnCl_2{\cdot}2H_2O$:NaCl) and replacing $SnCl_2{\cdot}2H_2O$ with $SnCl_4{\cdot}5H_2O$. Figure 3(a) shows the synthesized nanostructures when the amount of NaOH is reduced to half the reference conditions. The dimensions are significantly larger than were obtained for the reference sample. The SnO_2 nanoparticles have diameters greater than 100 nm. When the amount of NaOH is reduced, it is postulated that there is a subsequent decrease in the by-product NaCl which accounts for the increase in size observed. On the other hand, when the amount of NaOH is increased, nanoparticles of smaller dimensions (between ∼20 and 60 nm) were obtained (figure 3(b)). The chemical reaction that has taken place is as follows:

$$SnCl_2{\cdot}2H_2O + 2NaOH \rightarrow 2NaCl + 3H_2O + SnO.$$

The effect of varying the precursor to additive ratio on the dimension of the tin oxide nanoparticles was studied. Figures 3(c) and (d) show the nanostructures obtained when the ratio of precursor to additive (NaCl) was decreased and increased, respectively. It is observed that increasing the amount of additive results in nanostructures with reduced sizes. The diameter distribution is smaller (20–40 nm) as the size uniformity improves. This can be explained by the fact that the increased amount of NaCl and the water molecules produced can effectively precipitate to form a functional group which absorbs at the surface of the particles, thus inhibiting crystallite growth [7, 8]. Another important aspect of this designed

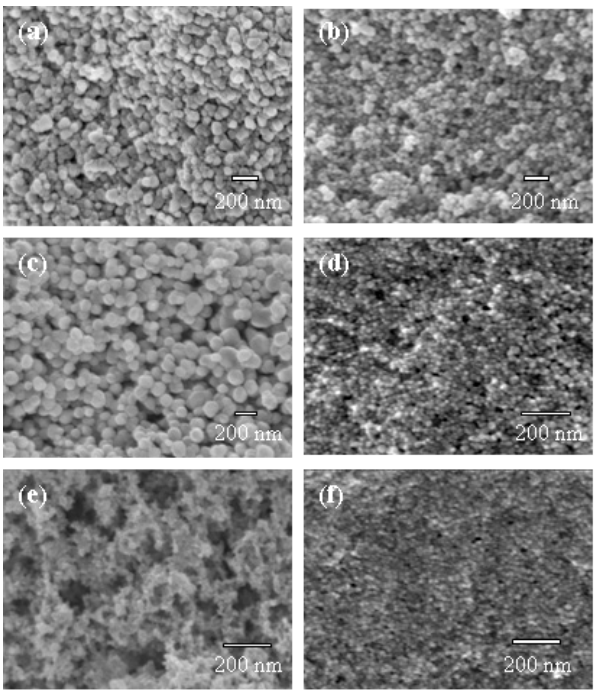

Figure 3. SEM images of the SnO_2 nanostructures obtained with ((a) and (b)) the precursor ratio decreased and increased, ((c) and (d)) the precursor to additive ratio decreased and increased, (e) $SnCl_2{\cdot}2H_2O$ replaced by $SnCl_4{\cdot}5H_2O$, and (f) the reaction temperature decreased.

solid-state reaction is the inclusion of NaCl additives. The particle size of the end product is easily controlled through the addition of NaCl or KCl additive [11–15]. Also, NaCl helps to separate the SnO_2 particles from agglomeration. After the reaction, the product mixture contains both the desired material and an alkali metal halide salt by-product which can be effectively removed via simple washing and rinsing. It has been noted that in the absence of NaCl additive, micron-sized agglomerated and non-uniform SnO_2 crystals have been obtained. Thus, it is evident that the NaCl additive is important in controlling the size and to prevent agglomeration of the nanoparticles [8, 11–15]. Likewise, the as-synthesized nanostructures increase in size to diameters of >100 nm as the NaCl additive is decreased to half the reference quantity.

Next, the tin precursor was replaced by the $SnCl_4{\cdot}5H_2O$; the corresponding chemical reaction is as follows:

$$SnCl_4{\cdot}5H_2O + 4NaOH \rightarrow 4NaCl + 7H_2O + SnO_2.$$

From the reaction equation, it is noted that the final amount of NaCl by-product is increased, which effectively produces smaller dimension nanoparticles, of 10–30 nm in diameter (figure 3(e)). It is also observed that the synthesized nanoparticles are not as closely packed as those produced by the $SnCl_2{\cdot}2H_2O$ precursor, rendering them porous in structure. This was later confirmed by the BET measurements.

Figure 3(f) shows the synthesized nanostructures when the annealing temperature was decreased by 50 °C. A decrease in temperature results in nanoparticles of smaller dimensions (∼20–40 nm diameter). The change in dimension of the

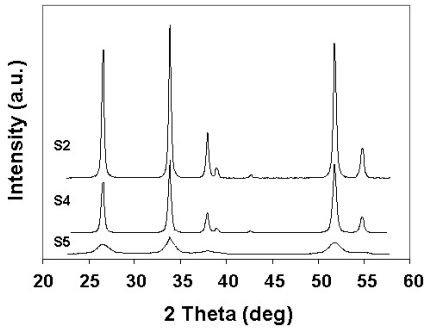

Figure 4. XRD spectra obtained for the S2 (40 nm), S4 (30 nm), and S5 (15 nm) samples.

nanostructures can be explained by the growth mechanism of the solid-state reaction employed. Penn *et al* reported that an oriented attachment growth mechanism is most evident in synthesis processes by which the reactive particles are aggregated and close-packed as is the case with a solid-state reaction [16]. The growth mechanism involves the unplanned self-organization and coalescence of neighbouring particles at a planar interface to form a larger structure [7, 16–18]. It is postulated that as the annealing temperature decreases, the frequency of collisions between the reactive particles is reduced, and this decreases the coalescence between adjacent particles, hence resulting in smaller nanostructures (diameter 20–40 nm). Similarly, we would expect that elevated temperature increases the frequency of particle collisions, which results in larger nanostructures. This has been experimentally verified, and the nanostructures grown at higher temperature (800 °C) have a larger diameter distribution of 200–300 nm. Table 1 summarizes all the experimental parameters investigated and the results obtained. It is noted that the annealing time has an insignificant effect on the dimension of the synthesized nanostructures.

The XRD spectra obtained for the synthesized nanoparticles with average diameters of approximately 15 nm (S5), 30 nm (S4) and 40 nm (S2) are shown in figure 4. All the XRD peaks observed are found to be consistent with those of bulk SnO_2 (JCPDS File No. 77-0450), thus reaffirming that the synthesized material is SnO_2. The diffraction peaks are observed to broaden as the particle size is reduced. The crystallite size (t) is calculated from XRD spectra using the well-known Scherrer formula [19].

$$t = \frac{K\lambda}{\beta \cos\theta}$$

where K is the Scherrer constant, β is the measured full width at half maximum (FWHM) in radians, θ is the Bragg angle of the diffraction peak, and λ is the x-ray wavelength (0.154 18 nm). The crystallite sizes of the SnO_2 nanoparticles were calculated to be 11, 28 and 36 nm. It is noted that there is a possibility of line width broadening due to lattice distortion and/or instrumental factors which could lead to an underestimation of crystal size.

Figure 5 shows the PL spectrum obtained for the S5, S7 and reference samples. It is known that the band gap of

Table 1. Summary of the effects of various reaction parameters.

Reaction parameters	Reference conditions	Reaction variations	Sample	Diameter of nanoparticles
Precursor ratio ($SnCl_2{\cdot}2H_2O$:NaOH)	1:2	1:1	S1	100–200 nm
		1:4	S2	20–60 nm
Precursor to additive ratio ($SnCl_2{\cdot}2H_2O$ + NaOH:NaCl)	1:2	1:1	S3	100–300 nm
		1:4	S4	20–40 nm
Tin precursor	$SnCl_2{\cdot}2H_2O$	$SnCl_4{\cdot}5H_2O$	S5	10–30 nm Increase in porosity
Annealing temperature	400 °C	350 °C	S6	20–40 nm
		800 °C	S7	200–300 nm
Annealing time	2 h	1 h	S8	No significant change
		4 h	S9	No significant change

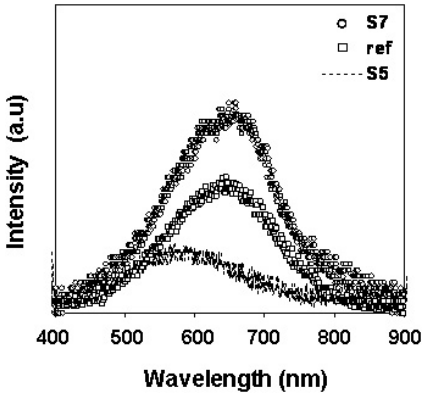

Figure 5. PL spectra of the reference, S5 and S7 samples obtained at room temperature.

SnO_2 is 3.6 eV [8]. Therefore, the excitation energy of a He–Cd laser (λ_{ex} = 325 nm = 3.82 eV) would be high enough to pump carriers to the excited states. Red emission at a wavelength of approximately 650 nm is observed for both S7 and reference samples. Since the band-to-band emission peak is not observed, it is very likely that the broad PL emission might be related to surface defects, oxygen vacancies and tin interstitials. The defects lead to the formation of a considerable amount of trapped states within the bandgap, resulting in red emission at room temperature. Although there is a similarity in the shape of the PL spectra for two samples, the emission intensity becomes stronger on increasing the synthesis temperature. As the diameter of the SnO_2 is decreased (S5), it is observed that broadening of visible emission bands and peak shifting occur. Sample S5 exhibits a weak yellow emission peak at ∼600 nm. It is known that a measured room temperature PL spectrum consists of a superimposed free-exciton peak and its phonon replicas [20]. The relative intensity of the dominating emission is determined by crystalline quality, which can lead to a spectral shift [20].

3.2. Hydrogen sensing

The hydrogen sensing properties of the SnO_2 nanostructures were measured between 200–500 °C by cycling between atmospheric air and 500 ppm H_2. It can be seen from figure 6(a) that the SnO_2 nanostructure sensor exhibits highly consistent responses over many cycles, which translates to high device stability. Figure 6(b) shows the sensitivity–temperature relationships obtained for different average particle sizes of 20 nm (S5), 30 nm (S4) and 40 nm (S2). The effective surface areas of all the samples (S5, S4 and S2) were measured using the BET method, and found to be 83.51, 46.81 and 19.09 $m^2\ g^{-1}$, respectively. It is observed that sensors made up of smaller nanoparticles possess higher gas sensitivities. This is due to the increase in effective surface area as the particle size decreases. The gas sensing mechanism of a SnO_2 sensor is based on surface reactions between the oxygen species and the reducing gas in contact with the sensor [21–23]. When the effective surface area of the sensor increases, it results in an increase in the number of surface adsorption sites, and hence an increase in the oxygen species available for reaction. This will translate to larger resistive changes for the sensor and hence result in higher sensitivities [24]. The relationship between the surface areas and maximum sensitivities was investigated, and was observed to be linear (figure 6(c)). It can be extrapolated that adjusting the material structure sizes and porosity are methods that can improve the gas sensing properties. However, both adjustments of structure sizes and porosity are basically attempts to increase the surface area of the sensor. This improvement, however, is a linear function, as proven in our studies as well as in other reports [24, 25], rendering it to be a rather ineffective method. Moreover, increased porosity also poses the issue of reduced device mechanical strength. A possibly superior method of improving gas sensing properties is via the approach of functionalizing SnO_2 nanostructures with noble metals. Thus, studies on the effect of Pd-coated sensors on the gas sensitivity were carried out. Pd was deposited on the same SnO_2 sensors on which gas sensing measurements were previously measured. This was to ensure that fair and controlled experiments were carried out.

Figure 6(d) illustrates the sensitivity–temperature relationships of the Pd-functionalized samples (S5, S4 and S2). The gas sensitivities were found to increase by approximately 1.5 times. The results show great potential in gas sensitivity improvement since it is noted that the Pd coating was done only at the surface of the whole pellet, which is approximately $<2\%$ of the total surface area of the SnO_2 nanoparticles that made up the pellet sensors. More work is now in progress to functionalize SnO_2 nanoparticles with Pd via a chemical route so as to ensure coating on each individual nanoparticle. The future

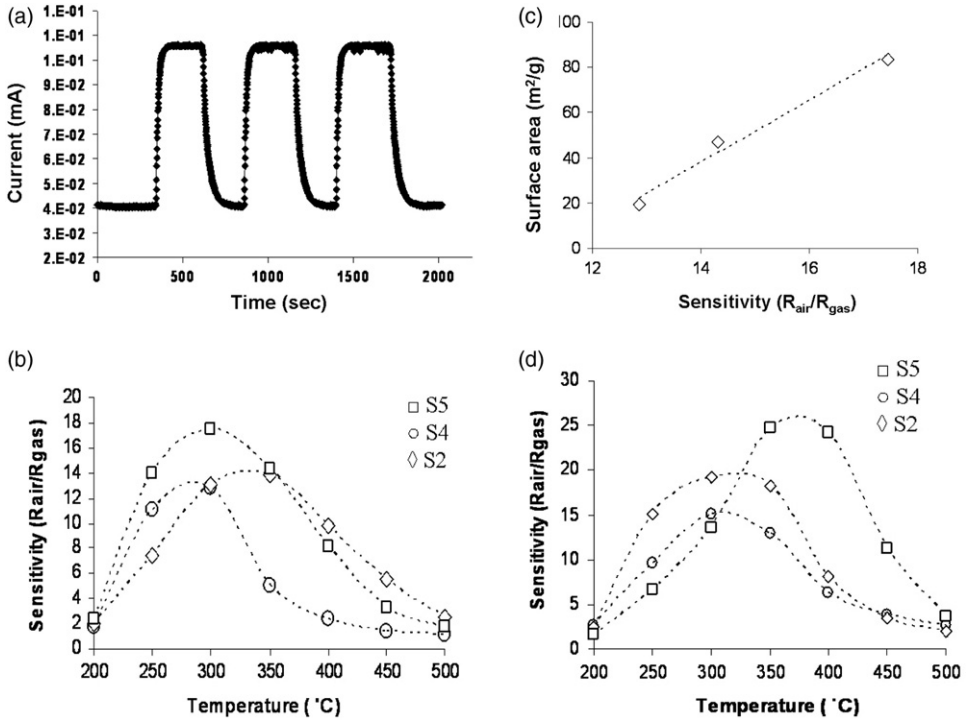

Figure 6. (a) Typical current response of a SnO_2 hydrogen sensor. (b) Sensitivity–temperature relationship before Pd functionalization. (c) Relationship between sensitivity and sensor surface area. (d) Sensitivity–temperature relationship after Pd functionalization.

work on optimization of Pd coating on nanostructures is important as it has been reported that Pd-based sensors have shown high sensitivity and selectivity towards hydrogen at room temperature [26]. The enhancement by Pd is most likely due to a 'spill-over' mechanism, wherein hydrogen molecules dissociate on the catalytic Pd clusters and then diffuse, probably across and/or through the clusters, to the substrate where the hydrogen atoms can interact with the semiconducting SnO_2 nanoparticles, to increase the conductance [27]. The conductance change is the result of adsorbed hydrogen atoms acting as donors to induce an accumulation layer by 'spilled-over' hydrogen atoms.

4. Conclusions

The controlled synthesis of high-yield and uniform size SnO_2 nanostructures has been successfully demonstrated. Hydrogen sensors made up of the SnO_2 nanoparticles were found to possess high sensitivity and stability. The Pd-functionalized SnO_2 nanoparticle based sensors produced show great potential for improved hydrogen detection sensitivity. Functionalizing sensors with various noble metals is believed to be a simple and cost-effective technique to improve the gas sensing properties in addition to the possibilities of utilizing specific catalytic, magnetic and optical properties of the noble metals.

Acknowledgments

The authors acknowledge the financial support of the National University of Singapore, research grants R-533 000 002 123 and R 533 000 003 112.

References

[1] Grimes C A *et al* 2003 A sentinel sensor network for hydrogen sensing *Sensors* **3** 69–82
[2] Wang C, Chu X F and Wu M M 2007 Highly sensitive gas sensors based on hollow SnO_2 spheres prepared by carbon sphere template method *Sensors Actuators* B **120** 508–13
[3] Kaur J, Kumar R and Bhatnagar M C 2007 Effect of indium-doped SnO_2 nanoparticles on NO_2 gas sensing properties *Sensors Actuators* B **126** 478–84
[4] Chacko S, Bushiri M J and Vaidyan V K 2006 Photoluminescence studies of spray pyrolytically grown nanostructured tin oxide semiconductor thin films on glass substrates *J. Phys. D: Appl. Phys.* **39** 4540–3
[5] Kang S K, Yang Y K and Mu J 2007 Solvothermal synthesis of SnO_2 nanoparticles via oxidation of Sn^{2+} ions at the water–oil interface *Colloids Surf.* A **298** 280–3
[6] Cho P S, Kim K W and Lee J H 2007 Improvement of dynamic gas sensing behavior of SnO_2 acicular particles by microwave calcination *Sensors Actuators* B **123** 1034–9
[7] Sun J Q *et al* 2006 Novel method for high-yield synthesis of rutile SnO_2 nanorods by oriented aggregation *Cryst. Growth Des.* **6** 1584–7
[8] Wiley J B and Kaner R B 1992 Rapid solid-state precursor synthesis of materials *Science* **255** 1093–7
[9] Deshpande A C *et al* 2006 Field emission from oriented tin oxide rods *Thin Solid Films* **515** 1450–4
[10] Chen D L and Gao L 2004 Novel synthesis of well-dispersed crystalline SnO_2 nanoparticles by water-in-oil microemulsion-assisted hydrothermal process *J. Colloid Interface Sci.* **279** 137–42
[11] Zhang D F, Sun L D, Xu G and Yan C H 2006 Size-controllable one-dimensional SnO_2 nanocrystals: synthesis, growth mechanism and as sensing property *Phys. Chem. Chem. Phys.* **8** 4874–80
[12] Li F, Xu J Q, Yu X H, Chen L Y, Zhu J M, Yang Z R and Xin X Q 2002 One-step solid-state reaction synthesis and

gas sensing property of tin oxide nanoparticles *Sensors Actuators* B **81** 165–9
[13] Yu X H, Li F, Ye X R, Xin X Q and Xue Z L 2000 Synthesis of cerium (IV) oxide ultrafine particles by solid-state reaction *J. Am. Ceram. Soc.* **83** 964–6
[14] Ye X R, Jia D Z, Yu J Q, Xin X Q and Xue Z L 1999 One-step solid-state reactions at ambient temperatures—A novel approach to nanocrystals synthesis *Adv. Mater.* **11** 941–2
[15] Li F, Yu X H, Pan H J, Wang M L and Xin X Q 2000 Syntheses of MO_2 (M = Si, Ce, Sn) nanoparticles by solid-state reactions at ambient temperature *Solid State Sci.* **2** 767–72
[16] Penn R L and Banfield J F 1998 Imperfect oriented attachment: dislocation generation in defect-free nanocrystals *Science* **281** 969–71
[17] Sophie M *et al* 2002 Synthesis and characterization of crystalline tin oxide nanoparticles *J. Mater. Chem.* **12** 2396–400
[18] Caue R, Lee E J H, Giraldi T R, Elson L, Jose A V and Leite E R 2004 Study of synthesis variables in the nanocrystal growth behavior of tin oxide processed by controlled hydrolysis *J. Phys. Chem.* **108** 15612–7
[19] Toney F, Gijo J, Siby M, Rejikumar P R and Unnikrishnan N V 2007 An ultra-low hydrolysis sol–gel route for titanosilicate xerogels and their characterization *J. Sol–Gel Sci. Technol.* **41** 163–8
[20] Ho G W and Wong A S W 2006 One step solution synthesis towards ultra-thin and uniform single-crystalline ZnO nanowires *Appl. Phys.* A **86** 457–62
[21] Gaggiotti G, Galdikas A, Kaciulis S, Mattogno G and Setkus A 1995 Temperature dependencies of sensitivity and surface chemical composition of SnO_x gas sensors *Sensors Actuators* B **25** 516–9
[22] Chung W Y, Kim T H, Hong Y H and Lee D D 1995 Characterization of porous tin oxide films and their application to microsensor fabrication *Sensors Actuators* B **24** 482–5
[23] Daoudi K, Sandu C S, Moadhen A, Ghica C, Canut B and Bessais B 2003 ITO spin-coated porous silicon structures *Mater. Sci. Eng.* B **101** 262–5
[24] Li G J, Zhang X H and Kawi S 1999 Relationships between sensitivity, catalytic activity and surface areas of SNO_2 gas sensors *Sensors Actuators* B **60** 64–70
[25] Li G J and Kawi S 1998 High surface area SnO_2: a novel semiconductor oxide gas sensor *Mater. Lett.* **34** 99–102
[26] Berlin C W and Sarma D H R 1993 Thick film sense resistor composition and method of using the same. Delco Electronics Corp. *US Patent Specification* 5221644
[27] Fryberger T B and Semancik S 1990 Conductance response of Pd/SnO_2 (110) model gas sensors to H_2 and O_2 *Sensors Actuators* B **2** 305–9